

An Optical Method for the Quality Exploration of a GaAs Material

Hilal Yücel KURT^{1,*}

Gazi University, Faculty of Sciences, Department of Physics, 06500 Ankara, Turkey

Received:27/08/2014 Revised:11/09/2014 Accepted:11/09/2014

ABSTRACT

The explorations on the surface qualities of these materials become very important for the preparation of solar cells in *PVs*. Therefore a nondestructive optical testing method is proposed in this paper by using *GaAs PV* materials. The proposed method uses a gas ionization system (*IS*) together with an optical measurement tool powered by the fractal dimension analysis (*OMT-FD*). The method initially records the spatial distributed light emission intensity (*SDLEI*) data radiated from the *IS* including the *PV* material and applies *OMT-FD* to this data in order to find out the optical properties of the sample. Thus the efficiencies of the discharge light emission (*DLE*) intensities can be accurately and qualitatively investigated and the optical responses of charge carriers are determined for any external voltage range. It has been proven that *OMT-FD* results indicate a sharp increment above a certain external voltage to *IS* and gives a quality value for the *PV* cells under the appropriate external voltage value applied to the *IS*. The optimized parameter set for the testing system has been ascertained.

Keyword: Quality exploration, GaAs, gas discharge, fractal

1. INTRODUCTION

Due to the environmental problems, population and economic growths, present energy perspective skips to much clean, carbon-free and renewable energy systems world-widely [1]. While the traditional energy resources lose their popularities, solar, tidal, wind and geothermal energy resources take interest for a much sustainable energy solutions. The main objective of present innovations on the energy issues is to develop new resources with environment-friendly, easy applicable, cost- and constructively- effective materials.

It has been known that solar energy or energy conversion through the photovoltaic (*PV*) cells [1,2] is one of the most preferred energy resources. For *PV* cells, the band gap of semiconductors can be adjusted by alloying them with appropriate materials by using

present laboratory conditions. The present band gap researches enable heterojunctions, which can be critical for the design of high-performance, efficient optoelectronic devices, which can be used as *PV* materials. At present, *PVs* which are widely used in many solid-state applications are usually made of semiconductors, such as *Si* [3], *GaAs*, and so forth. Developments of thin-film photovoltaic devices, which can yield to sufficient efficiency, are expected to reduce the cost of the material production. On the other hand, a reduction in the thickness of the photoactive device material inevitably makes the photon absorptivity of the semiconductor poorer and results in a low electric output [4]. Because of its higher electron mobility, low power consumption, high breakdown field and the direct band gap, *GaAs* is one of the most promising materials for *PV* industry [5]. In this manner, there exists much interest in multi-junction/intermediate band

*Corresponding author, e-mail: hkurt@gazi.edut.tr

devices produced by *GaAs* based alloys for the higher efficiency in *PV* systems. *GaAs* solar cells retain the efficiency record for the single junction *PV* cells. The enhancement in *GaAs* solar cell efficiency is therefore important to improve solar cell power. One should also underline the attempts on inclusion of quantum wells into *GaAs* material as semiconductor hosts. These attempts would be the best options for the increment of efficiency for the solar cells [6]. In addition, *GaAs* has many attractive features with ideal direct band gap energy of 1.43 eV and it is highly absorptive and relatively insensitive to heat. The last feature is vital; since Sun-caused overheating of *PV* materials can cause certain damages and fires on the *PV* panels. On the one hand, *GaAs* can be alloyed with many materials such as aluminum, phosphorus, indium, etc. and has longer lifetime and high efficiency [1,2]. Apart from the laboratory and house-hold applications of *GaAs PVs*, the radiation resistance makes *GaAs* suitable for both concentrator applications and satellite devices in space, too [7].

In the manufacturing process, *GaAs* material production is much basic compared to the silicon material production due to its selective-area isolation [1]. The operation of the *GaAs* device can be realized at higher power levels than the equivalent silicon devices, since it has much higher breakdown voltage U_B . *GaAs* allows a thinner cell, providing material and weight savings when its relatively high absorption coefficient is considered [8]. Recently, there exist a number of researches on the electrical and photovoltaic properties of the *Au/n-GaAs* Schottky diodes in order to understand the possibility of their use in innovative *PV* applications [8]. Although the fixed surface charge and the interface states affect the bias characteristics of Schottky devices in reverse and forward directions [9], they are not the total factors to construct a good *PV* cell. In fact, the enhancement of the optical features of *PV* materials can lead to better performance and reliability for solar applications [10]. In addition to their electrical features, on the other hand, next-generation *PVs* are planned to be in an array configuration, namely the semiconductor nanowire array (*NWA*) [11-13] because of their lower cost and higher efficiency of energy conversion compared to the conventional thin film materials [14-17]. *GaAs NWs* show interesting behaviors such as better electrical and optical properties among the other *III-V* materials. The direct band gap and high absorption coefficient of *GaAs NWs* make them a good candidate for the production of future *PV* materials, too [12,13]. In some recent studies, many advances have been reported on the production of *GaAs NW* solar cells. Czaban et al. observed a *PV* effect with a photo-conversion efficiency up to 0.83%, when the vertically oriented *GaAs NWs* have been grown on the *n-GaAs* (111)B substrates [12]. In other study, Colombo et al have reported a coaxial pin single nanowire cell with 4.5% efficiency [13]. This increasing trend in the efficiency of the *GaAs NWs* is promising for the *PV* material improvement.

As an optical testing facility- an ionization system (*IS*) includes a discharge cell with anode and cathode

structures. The difference of the optical test system from the all other plasma systems is that cathode is made up by the *PV* material, which will be tested. From the point of *IS*, if one of the electrodes is considered as a semiconductor plate; the gas discharge current flowing from the anode to the semiconducting cathode is distributed over the total area of the specimen at the cathode and the semiconducting electrode produces a discharge light emission (*DLE*) over the electrode surface [17-18]. The intensity and the homogeneity of *DLE* strictly depends on the resistivity distribution of the semiconductor plate (i.e. *PV* material existing at the cathode), and the *DLE* intensity becomes proportional to the discharge current. Even a spatially inhomogeneous infrared (*IR*) light distribution is projected on the surface of the semiconductor plate from an external light source; this would also affect the spatial resistivity distribution in the semiconductor sample existing at the cathode. The measurements made with or without external infrared excitation will give a qualitative result on the quality of *PV* materials by measuring the spatial resistivity and optical feature of the sample. Even the time-dependent local changes of the *DLE* can be observed via this *IS* and the resistivity differences through the entire area can be identified clearly. Following the basic optimization process, the *PV* material can be tested in terms of its surface qualities by following the *DLE* as a result of resistivity distributions [19-21].

In the present work, an optical method is proposed to measure the quality of a *GaAs* material. The specimen is put into the discharge cell under a certain gas and the optical measurements are made spatially and temporally in order to examine the discharge light emission (*DLE*) intensities. While the gas structure assists to adjust the appropriate voltage in order to produce the *DLE* and an observable current between the electrodes of the ionization cell, the *DLE* data are transferred into the optical measurement tool powered by the fractal dimension analysis (*OMT-FD*). This paper also includes the optimization studies by adjusting the correct voltage, pressure and electrode distance to the test facility. The paper content is summarized as follows: Section 2 gives the experimental details on the measurement of *DLE* data. Section 3 draws a background on fractal dimension calculation. The main part - Section 4 mentions about the optimization process and test results. Finally the concluding remarks are presented at the last section.

2. EXPERIMENTAL

A sample photo of the nondestructive photovoltaic test system is shown in Fig. 1(a). The main part of the system is the discharge cell given by No. 4 (Fig. 1(a-c)), where the photovoltaic test material is situated at the cathode. From right hand-side to the left, the total testing system includes an external light source (1), optical lens (2) for visible light emitted from (1), silicon filter (3), discharge cell (4), *CCD* camera (5), vacuum pump (6), vacuum valve (7), facility box (8) and digital manometer (9).

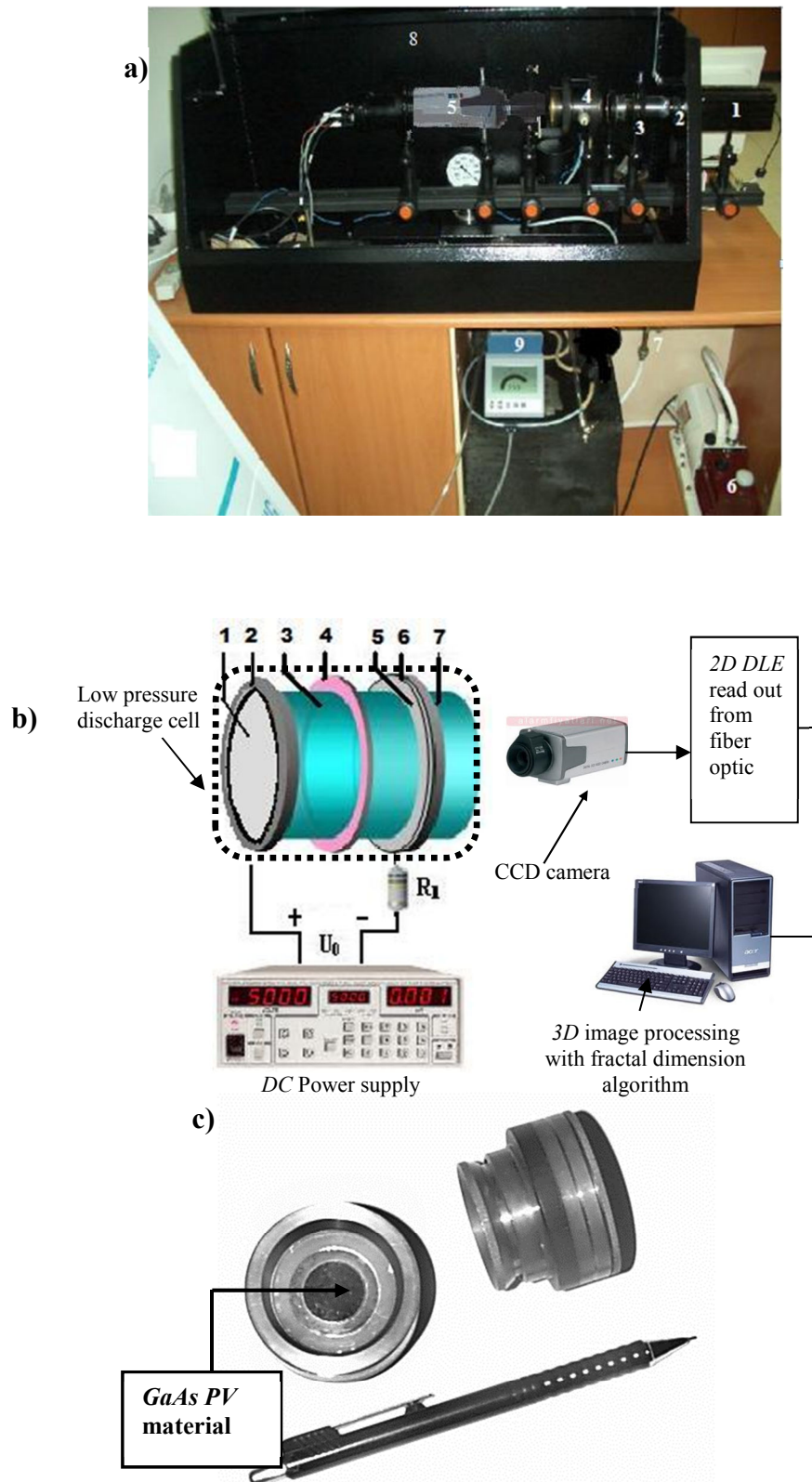


Fig. 1. (a) A photo of photovoltaic test system: 1- Light source; 2-optical lens; 3- Silicon filter ;4- gas ionization system (IS); 5- CCD camera; 6- vacuum pump; 7-vacuum valve; 8-facility box and 9-digital manometer ; (b) Experimental setup including an ionization cell. Numbers indicate: 1- *GaAs* PV material; 2-specimen holder; 3- adjustable discharge gap; 4-insulator foil (mica); 5-transparent conductor (*SnO*₂); 6- flat glass disc, 7- visible light beam. The dashed part of (b) is shown in (c). The *GaAs* photovoltaic material is at the middle of the cell. Interelectrode distance d (in μm) is between *GaAs* PV material and transparent *SnO*₂ conductor.

A PC gets the discharge light emission from the CCD camera (ITIC equipped with a proximity focused Gen II image intensifier coupled to the charge coupled device (CCD) via a tapered fiber optic) as shown in Fig. 1(b). For the electrical features of a DLE, a PC and the interface equipments are used to record the current-voltage characteristics (CVC) of an individual DLE in addition to the DLE patterns of the photovoltaic material. The plasma current I and the voltage values on the electrodes are measured synchronously by a multimeter (Keithley 199) and digitalized by a custom-made software in PC (Fig1(b)). The system uses a voltage supply of Stanford PS 325 for the voltage adjustment. In the case of optical excitation of the photovoltaic sample, the test system can also be used under different infrared light (IR) in order to excite the electronic states of the PV samples.

In that case, the photocathode can be illuminated by an incandescent lamp with 250 W in front of the cathode uniformly. Therefore the photoconductivity of the sample can be increased up to a certain level. The illumination intensity L_p can be varied between 10^{-6} Wcm^{-2} and 10^{-2} Wcm^{-2} by the use of filters. Between the incandescent lamp and the sample, there exists a Si-filter, which transmits the wavelengths between 0.9 μm and 1.6 μm . The maximum illumination is measured as 8×10^{-2} Wcm^{-2} . Diameter of the effective electrode area of GaAs PV material D is 22 mm. The discharge gap d (between 30 μm and 525 μm) and the pressure p (between 15 Torr and 550 Torr) are adjusted to provide a bright DLE even at low current densities. Thus, that causes an efficient emission process because of charged particles emitted from GaAs PV material under certain applied voltage. The CVCs are recorded for different voltages within a rate of 5 Vs^{-1} . The plasma current is obtained by measuring the voltage on a load resistance of 10 k Ω series to the cell. The discharge stability is provided by using a set-up with a thin adjustable gap d . The DLE can be measured using a photon counting unit ELSEC - 9010 from Littlemore Sci. Eng.

For the implementation of quality tests, dark operation is mainly used in order to observe the discharge mechanism of the material with natural electronic states. The voltage applied to the discharge cell can be increased step by step from 200 Volt to 2.5 kV in order to see the response of the photovoltaic material under different discharge conditions. It should be pointed out that the software can record the DLE patterns successively, when the applied voltage is increased step by step. However, a constant voltage can also be used for a certain time span in order to get a detailed DLE for the 3D processing. After the 2D DLE pattern is sent to the PC, 3D pattern is created by the software package (Image pro Plus) [22] and the gray numbers over the entire DLE surface is ascertained for the fractal dimension (FD) analysis.

3. BACKGROUND ON OPTICAL MEASUREMENT TOOL POWERED BY FRACTAL DIMENSION ANALYSIS (OMT-FD)

The fractal dimension (FD) technique has been used for the material surface explorations in different disciplines. Some introductory papers of the author can be read in Ref. [23-26]. From the point of material explorations, a recent paper of Chen et al [27] can be given. The authors have reported the nanofractal structures in some Ge crystals and the fractal dimensions have been calculated for different annealing temperatures. In a different paper, Stoliar et al [28] investigated the fractal structures after the electron beam lithography to the Si samples. In addition, fractal analyses of atomic force microscopy (AFM) patterns of InGaN materials were calculated by Lam and Ji [29]. In these studies, the surface qualities of the semiconductor materials were analyzed by using the fractal approach.

Fractal is defined as a geometric object having a Hausdorff-Besicovich dimension, which exceed its discrete topological dimension [23-25]. The metric properties of a fractal object require a dimension value which is larger than its expected value [30]. It means that if the object is a line, the fractal dimension should be less than 1, whereas if the object is a surface, the dimension should be between 1 and 2. Basically, the technique is strictly related to the measurement approach. For example, the length measurement of a coastline can change with the measuring scale e and similarly, in a 2D plane, the total area on a surface can be calculated by using all the points with the same property using the measuring scale. Therefore, this coastline length L can be measured different just by adjusting various e values. When the measurement tool e gets smaller, L increases further since it can get the measurement in a much sensitive way [22-24]. This measurement process can be summarized by

$$L = ae^{-D_f} \quad (1)$$

Note that here a and D_f give real numbers and e is not the natural logarithm basis, in fact e is the scaling unit. Consequently, the fractal dimension of this coastline can be found by the logarithmic expression by taking the logarithm. It is denoted by D_f and the least squares linear fit of the \log values yield to the correct value:

$$D_f = - \frac{\log L}{\log e} \quad (2)$$

Note that since a is constant, we neglect it in Eq. 2. For a generalization, while a line has 1D, the dimension D_f of a fractal trace on any plane can be a continuous function between 1 and 2. In the same way, a planar curved surface is two-dimensional, while a fractal volume can have the dimension between 2 and 3 inside a volume.

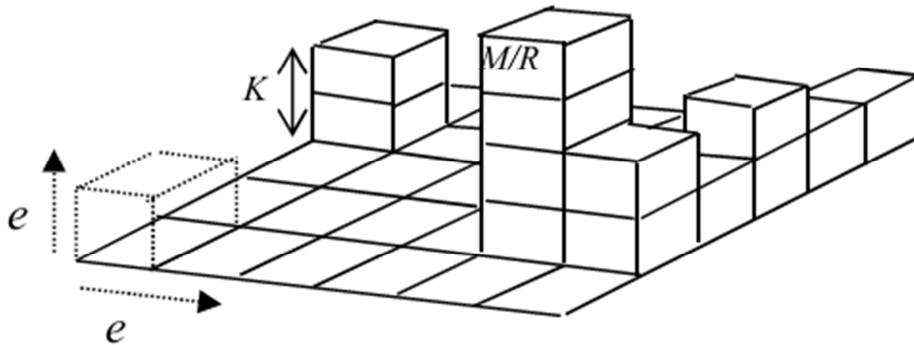


Fig. 2. The fractal dimension measurement of the sample surface via box counting.

There exist a number of methods to measure the dimension [23-25]. The box-counting method is the most applied one among them. It is developed by Gangepain and Roques-Carnes to analyze the pixel-based images [31]. This method has also become a basis for other techniques introduced by recent researchers studying image analysis [23-25]. The present authors also used this technique to identify the fractal dimension of the patterns obtained from an image converter [see Ref. 23-25]. For the box-counting method, Eq. 2 should be extended for an $M \times M$ sized image.

If grids which have $R \times R$ area are considered, the entire discharge pattern can be covered by the boxes having the sides $R \times R \times R'$ in the vertical direction (Fig. 2). If the image intensities (i.e. gray levels) are determined with a quantization over the whole volume as in Fig. 2, R' determines the number of boxes which contain at least one gray level intensity (i.e. *DLE* intensity). $R' = R \times \frac{K}{M}$ is the multiplication of the gray level units and K gives the total number of gray levels with the maximal value of 256.

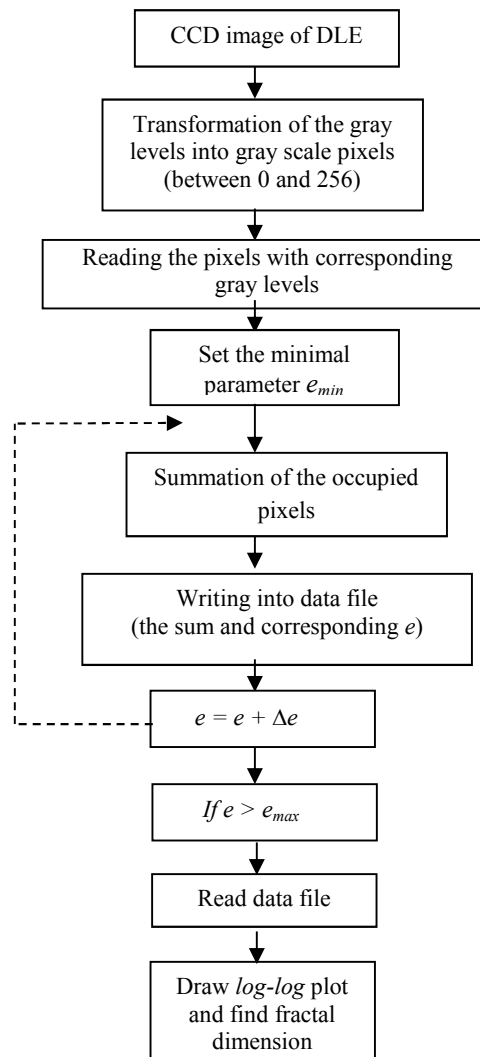


Fig. 3. The algorithm for the fractal dimension measurement.

The total number of boxes is used to identify the function L . Note that at least one gray level intensity on the entire surface contributes to this function. In order to determine the resulting dimension of an individual 3D pattern, one should adjust various R values as $e = \frac{R}{M}$ in terms of Eq. 2. Then

$L(R) \propto R^{-D_f}$ is found and the final expression can be obtained as a tangential value of the log-log plot,

$$D_f = -\frac{\log L(R)}{\log R} \quad (3)$$

$L(R)$ gives the summation of occupied pixels of the pattern and it is re-calculated for each R . A detailed algorithm for

this process is given in Fig. 3 for the numerical procedures. After the record of patterns this algorithm is applied to the patterns. The slope of the linear fit line yields to $-D_f$ as also indicated in Eq. 2.

4. RESULTS AND DISCUSSION

4.1. Optimization of DLE test facility

The discharge light emission (DLE) intensities for various applied voltages and current responses of the GaAs PV specimen are shown in Fig. 4.

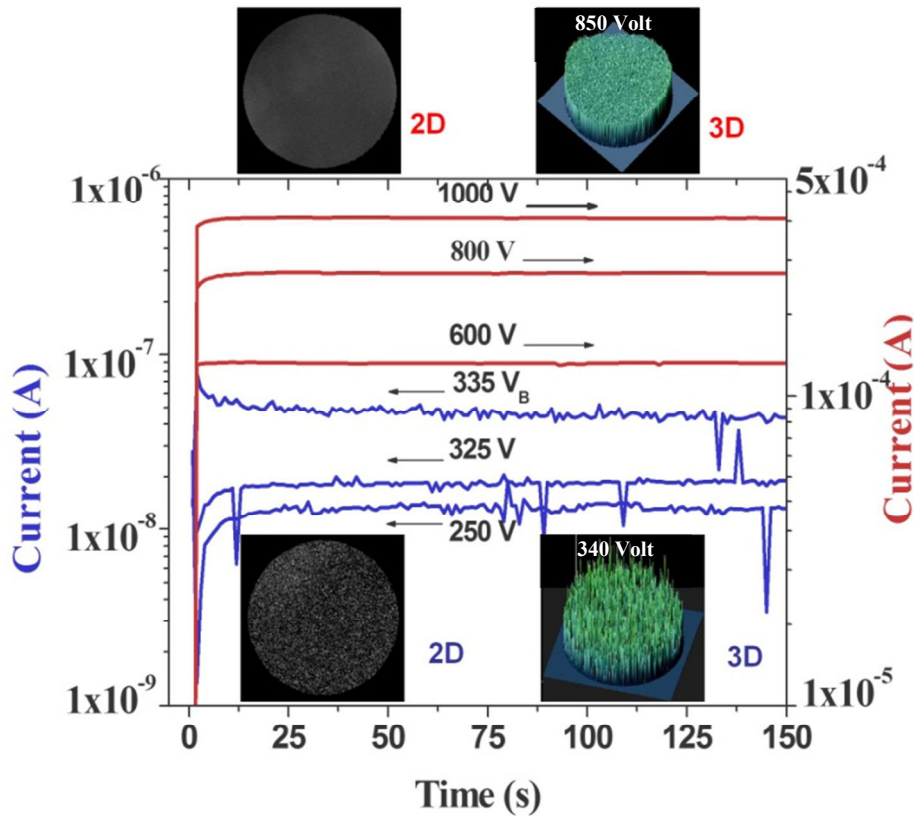


Fig. 4. Optimization of the current -voltage scaling by applying various voltages to the discharge cell for the detection of the measurement range of the specimen. $p = 100$ Torr, $D = 22$ mm and $d = 100 \mu\text{m}$. While the red plots correspond to the stable Townsend regime with the right-hand side scaling, the blue plots correspond to unstable pre-Townsend regime with the left-hand side scaling.

This figure proves that the applied voltage plays an important role in order to produce a homogeneous pattern from the photovoltaic material. Strictly speaking, the pattern becomes much homogeneous in terms of *DLE* beyond the breakdown voltage V_B which is found about 335 V. Beyond this voltage, the current flowing through the *PV* material becomes at the order of 0.1 mA. However the inhomogeneous *DLEs* are observed around the current value $0.1 \mu\text{A}$. While the 2D pattern of *DLE* and its 3D appearance below the current lines are observed at the breakdown voltage around 340 V, the patterns above the current lines belong to 850V. Before the quality measurement, an optimization test

should be carried out for the determination of the stable regime. It is obvious that the applied voltage 600-850 V to the discharge cell is sufficient for the optical measurement of *PVs*, since the temporal behavior of plasma current becomes stable.

The optimization does not only depend on the current flowing through the *PV* or the applied voltage to the discharge cell. In addition, the distance between the *PV* material and anode of the discharge cell d is also important for the optimization of testing procedure. In order to prove it, Fig. 5 is produced for various distance values between $45 \mu\text{m}$ and $525 \mu\text{m}$.

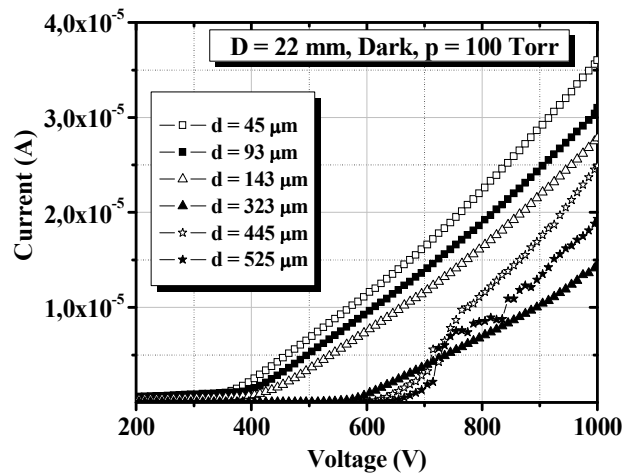


Fig.5. Optimization of the distance between the PV sample and anode.

It is clear that the current-voltage plots are much stable, when d is adjusted between $45\ \mu\text{m}$ and $143\ \mu\text{m}$. Further distances cause differences in resistance of the discharge system due to the plasma behavior inside the cell. Another important point is that there exist no current below the breakdown voltage. This plot also proves Fig. 4 in terms of current-voltage relation.

Fig 6 describes the current behavior as function of pressure in two cases of operation voltage. The upper curve is obtained for $U = 850\text{V}$ and the lower curve with open circles is obtained for the breakdown voltages of each pressure value. In the gas discharge systems, the breakdown voltage changes, when p is changed [16-21]. Therefore the breakdown voltages change around 335V for the investigated system. It is obvious from Fig. 6 that the current values decrease as function of pressure (p) at high voltages such as $850\ \text{V}$, which give smooth DLE patterns. However, the current

values which determinate the lowest values for the corresponding breakdown voltages at the specific pressures increase slightly as function of p around 335V , where the unstable and inhomogeneous patterns are observed as seen in Fig7a. The gray colored region between these two curves determines the quasi-stable and stable regions for the current. It means that the test system can operate at the stable voltage values from the upper threshold line of quasi-stable to the line of $850\ \text{V}$ in Fig.6.

In addition, if the voltage values are high enough, pressure of the discharge cell does not affect the optimized DLE in a large range between 25 and $550\ \text{Torr}$ according to the stable area in Fig. 6. This situation also gives an opportunity to measure the quality of the PV surface at high pressures by using specific system parameters.

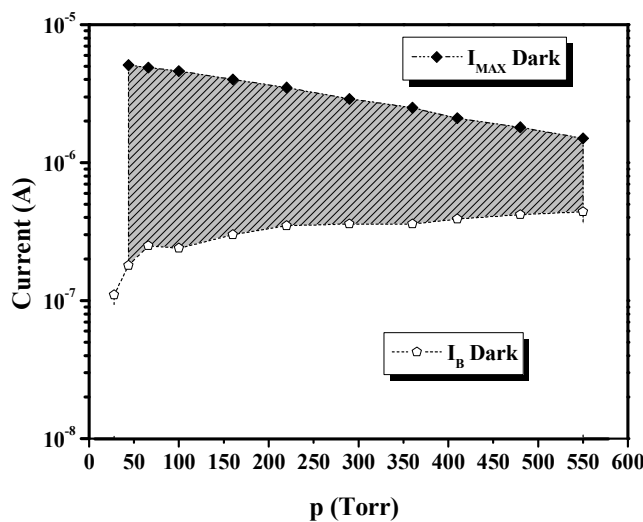


Fig. 6. The relation of discharge cell pressure and current flowing through the PV material for the currents at breakdown voltages (around 335V) and high (850V) voltage regimes, the combination of the quasi-stable and stable operation areas shown by gray color can be achieved between these two current regimes.

4.2. Optical measurements of photovoltaic material

In this subsection the optical measurements are taken and evaluated by using the proposed method. Fig. 7 represents the quality results of a PV material at different discharge potential.

The dimension value D_f for each DLE of PV pattern is found from the least-square linear fit of the box counting method as stated in the previous section. According to the slopes in these plots, the dimension values are summarized in Table 1.

The DLE intensities taken at 340V and shown in Fig. 7(a) has the minimal dimension value with $D_f = 2.33$. This value does not give the real quality of the PV

material, since the breakdown voltage U_B is around 335V and a homogeneous plasma structure cannot be obtained at this discharge voltage. When the voltage is increased further, the dimension values increase, too. Beyond 450V, the discharge becomes homogeneous due to the Townsend discharge regime which dominates the discharge process at the higher voltages than the breakdown voltage. According to Fig. 7(a-c), the dimension values are low before the Townsend region (see Ref. [20]). This result is reasonable, since the applied voltage cannot excite the entire area of the PV material. In other words, some areas which have slightly low resistivity values contribute to the DLE. For the higher resistivity areas, much higher voltages are required to excite.

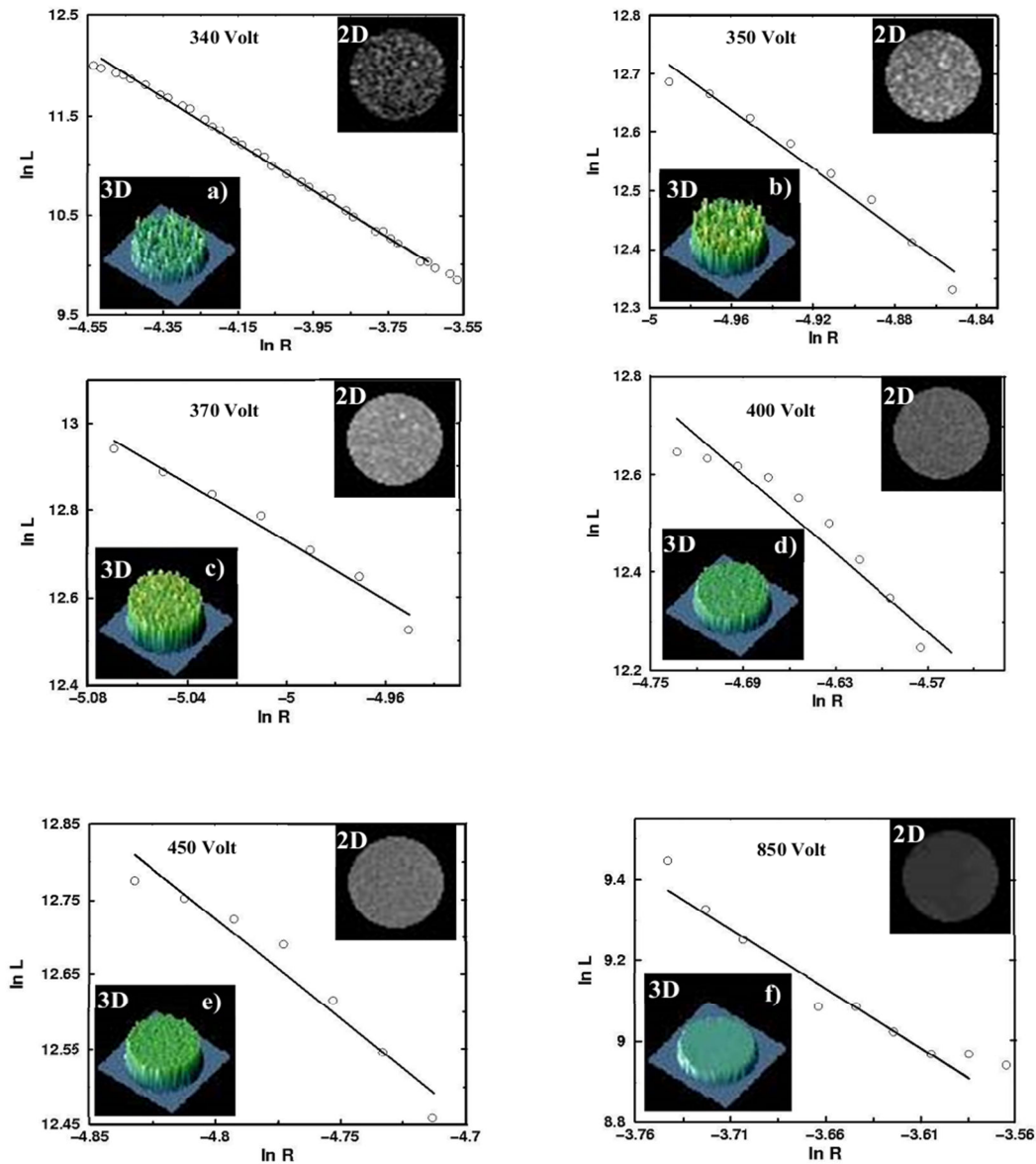


Fig.7. The 2D and 3D patterns and the log-log plots of 3D patterns at different discharge voltages. $p = 100$ Torr, $D = 22$ mm and $d = 100 \mu\text{m}$.

At this point, it becomes important to state that the manufacturing features and the spatial homogeneity of the *PV* plate play important roles. In addition, the impurities have already been found as key factors to affect the quality of some photocathodic semiconducting plate in the earlier studies [23-27]. Contrary to Fig. 7(a), Fig. 7(f) has a homogenous structure and nearly the all pattern grays are filled at

$U=850V$. When the spatially conducting condition is satisfied for the ionization cell, almost the entire surface of the *PV* becomes bright. The applied voltage excites almost the entire surface of the plate due to the fact that it is sufficient to overcome the higher resistivity surfaces of the *PV*. At that time the dimension values indicate sharp increase as seen in Table 1.

Table 1. The fractal dimension analysis of *DLE* patterns.

Pattern	U=340V Fig.7(a)	U=350V Fig.7 (b)	U=370V Fig 7(c)	U=400V Fig 7(d)	U=450V Fig 7 (e)	U=530V	U=580V	U=750V	U=850V Fig 7 (f)
Fractal dimension (D_f)	2.33	2.55	2.78	2.68	2.76	2.60	2.67	2.62	2.93

This voltage gives an opportunity to measure the surface quality of the *PV* materials. When the appropriate experimental parameters are adjusted to the system, the system can measure the quality of *PVs* via the fractal dimension analysis of *DLE*, quantitatively.

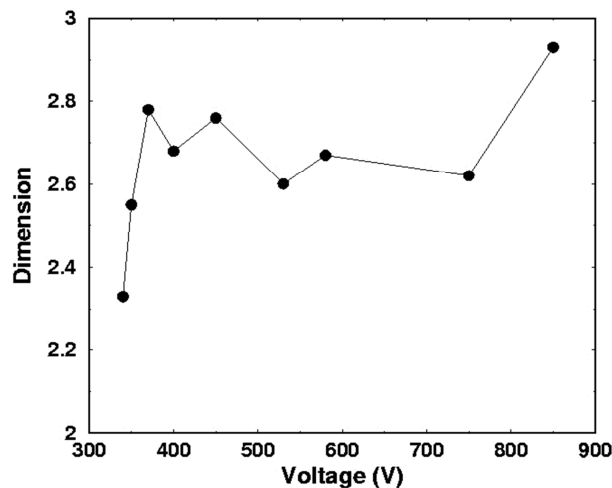


Fig 8. The fractal dimension values as a function of discharge voltage.

The most interesting region in Fig. 8 is the region between 450-750 Volts where the dimension values slightly fluctuate between 2.8 and 2.6. In these voltages, some parts of the *PV* material surface are too much excited, but some other regions are not excited and do not produce any *DLE*. Such higher voltages may increase the movement of the carriers inside the lower resistivity regions of the sample and this situation causes a non-homogenous *DLE* intensity over the plate. When the voltage is increased up to 850V, the resistivity regions do not play an important role and the surface quality of the sample only affects the results. In addition, the surface quality increases, when the dimension values increase near $D_f=3$. Thus, one can easily identify the dimension values as the optical quality identifier at various applied voltages and decide

on a qualitative result for the *PVs*. In order to have a better surface quality, the sample should indicate higher dimension values at lower applied voltages. The optimized parameters are found to be $(U,p,d) = (600-850V, 100 \text{ Torr}, 45 \mu\text{m})$ for the measurements and the same parameter set should be used for the whole samples, since the discharge light emission intensities and plasma currents change drastically by the parameters. In this case, the parameters which yield to lower dimension values cannot be accepted as the optimized parameter set. Because these values do not indicate the real surface quality due to the fact that the lower voltage values (i.e. 335V-600V) corresponds to the quasi- stable regime, where the most of charged particles of *PV* material are not included at the discharge process. However at $U = 600V$ and beyond

this value, the current I and DLE intensities become extremely stable. Therefore the optimized system parameters can be adjusted to these values. According to our earlier analyses on different samples (see in [24], $U = 600-850$ V has also been used for the quality measurements of different samples with surface distortions and those findings are also parallel to our new findings with PV samples.

5. CONCLUSIONS

An optical method has been proposed for photovoltaic materials via the fractal dimension. The system reads out the discharge light emissions and converts them to the $3D$ patterns for the evaluation of fractal dimension analysis. Thus, the quality of the materials can be tested by the comparison of dimension values belonging to each material at the optimized voltage value. The effects of pressure, voltage and sample-anode distance have also been clarified at this testing system. It is found out that the applied voltage for the discharge cell plays a very important role to produce efficient light emission intensities. Besides, while the pressure does not affect the DLE intensities too much, sample-anode distances smaller than $150\mu\text{m}$ gives much stable operation with a smooth discharge current.

ACKNOWLEDGEMENTS

This work was supported by Gazi University *BAP* research projects 05/2012-47, 05/2012-72.

REFERENCES

- [1] Jothilakshmi R, Ramakrishnan V, Kumar J, Saruac A, Kuballe M 2011 Micro-Raman analysis of GaAs Schottky barrier solar cell *J. Raman Spectrosc.* 42 422–428.
- [2] Subramanian B, Sanjeeviraja C 2002 Review of the compound semiconductors useful for photoelectrochemical solar cells *Bull. Electrochem.* 18 349-366.
- [3] Dallas W, Polupan O, Ostapenko S 2007 Resonance ultrasonic vibrations for crack detection in photovoltaic silicon wafers *Meas. Sci. & Technol.* 18 852–858
- [4] Harada Y, Imura K, Okamoto H, Nishijima Y, Ueno K, Misawa H 2011 Plasmon-induced local photocurrent changes in GaAs photovoltaic cells modified with gold nanospheres: A near-field imaging study *J. Appl Phys.* 110 104306 -104306-7.
- [5] Kundu S, Kumar A, Banerjee S, Banerji P 2012 Electrical properties and barrier modification of GaAs MIS Schottky device based on MEH-PPV organic interfacial layer *Mat Sci Semicon Proc.* 15 386–392.
- [6] Courel M, Rimada J C, Hernandez L 2012 An approach to high efficiencies using GaAs/GaInNAs multiple quantum well and superlattice solar cell *J. Appl. Phys.* 112 054511-18.
- [7] Ruzinsky M, Saly V 2001 Characterisation of selected GaAs thin film structures for concentrators *Acta Phys. Slovaca.* 51 45-52.
- [8] Hacke P, Uesugi M, Matsuda S 1994 A study of the relationship between junction depth and GaAs solar cell performance under a 1 MeV electron fluence *Solar Energy Materials and Solar Cells.* 35 113-119.
- [9] Zeng J J, Tsai C L, Lin YJ 2012 Hybrid photovoltaic devices based on the reduced graphene oxide-based polymer composite and n-type GaAs *Synthetic Metals.* 162 1411–1415.
- [10] Guo H, Wen L, Li X, Zhao Z, Wang Y 2011 Analysis of optical absorption in GaAs nanowire arrays *Nanoscale Res Lett.* 6 617-623.
- [11] Czaban J A, Thompson D A, LaPierre R R 2008 GaAs core-shell nanowires for photovoltaic applications. *Nano Lett.* 9 148-157.
- [12] Colombo C, Hei M, Grätzel M, Fontcuberta A M 2009 Gallium arsenide p-in radial structure for photovoltaic applications. *Appl Phys Lett.* 94 73108-73113.
- [13] Garnett E, Yang P D 2010 Light trapping in silicon nanowire solar cells. *Nano Lett.* 10 1082-1087.
- [14] Zhu J, Yu Z, Burkhard G F, Hsu C M, Connor S T, Xu Y, Wang Q, McGehee M, Fan S, Cui Y 2009 Optical absorption enhancement in amorphous silicon nanowire and nanocone arrays. *Nano Lett.* 9 279-282.
- [15] Hu L, Chen G 2007 Analysis of optical absorption in silicon nanowire arrays for photovoltaic applications *Nano Lett.* 7 3249 -3252.
- [16] Li J S, Yu H Y, Wong S M, Li X C, Zhang G, Lo G Q, Kwong D L 2009 Design guidelines of periodic Si nanowire arrays for solar cell application *Appl Phys Lett.* 95 243113-24116.
- [17] Kurt H Y, Sadiq Y, Salamov B G 2008 Nonlinear electrical characteristics of semi-insulating GaAs *Phys. Status. Solidi.A.* 205 321-329.
- [18] Salamov B G, Kurt H Y 2005 Current instability in a planar gas discharge system with a large diameter semiconductor cathode *J. Phys. D: Appl. Phys.* 38 682-687.
- [19] Sadiq Y, Kurt H Y, Albarzanji A O, Alekperov S D, Salamov B G 2009 Transport properties in semiconductor-gas discharge electronic devices *Solid-State Electron* 53 1009-1015.
- [20] Kurt H, Cetin S, Salamov B G 2011 Townsend Instabilities in a Modified Discharge System With

- Coupled Narrow Gaps *IEEE Transaction on Plasma Science* 39 1086-1091.
- [21] Kurt E, Kurt H, Bayhan U 2009 Ionization effects and linear stability in a coaxial plasma device *Cent Eur J Phys.*7 123-129.
- [22] Kurt H Y, Salamov B G 2007 Nonlinear transport of semi-insulating GaAs in a semiconductor gas discharge structure *Physica Scripta.* 76 641-648.
- [23] Kurt H Y, Kurt E, Salamov B G 2004 Fractal processing for an analysis of the quality and resistivity of large semiconductor plates *Cryst. Res. Technol.*39 743-753.
- [24] Salamov B G, Kurt H Y, Kurt E 2003 An analysis of the spatial homogeneity of a photodetector surface in an infrared image converter using the fractal dimension *Imaging Sci J.* 51 187-197.
- [25] Kurt H Y, Kurt E, Salamov B G 2006 Identification of the dynamics of plasma -induced damage in a CuInSe₂ thin film by fractal processing *Cryst. Res. Technol.* 41 698-707.
- [26] Akos N, Miklos M, Laszlo D, Gyozo B 2002 Morphological investigation of the electrochemically etched GaAs (001) surface *Materials Science and Engineering B* 90 67.
- [27] Chen Z, Li Q, Pan D, Zhang H, Jiao Z, Wu M, Shek C H, Wu C M L, Lai J K L 2011 Polycondensation-type Ge nanofractal assembly *Materialstoday.* 14 106-113.
- [28] Stoliar P, Calo A, Valle F, Biscarini F 2010 Fabrication of Fractal Surfaces by Electron Beam Lithography, *IEEE Transaction on Nanotech.*9 229 - 236.
- [29] Lam K T, Ji L W 2007 Fractal analysis of InGaN self-assemble quantum dots grown by MOCVD *Microelectron J.* 38 905-909.
- [30] Mandelbrot B B 1982 *The Fractal Geometry of Nature* (Freeman Press, San Francisco, CA)
- [31] Gangepain J J and Roques C 1986 Fractal approach to two-dimensional and three dimensional surface roughness *Wear.*109 119-126.